A lytic transglycosylase connects bacterial focal adhesion complexes to the peptidoglycan cell wall

Carlos Ramirez Carbo[1, 2, 3], Olalekan G. Faromiki[1, 3] and Beiyan Nan[1*]

[1] Department of Biology, Texas A&M University, College Station, TX 77843, USA

[2] The Genetics and Genomics Interdisciplinary Program, Texas A&M University, College Station, TX 77843, USA

[3] C. R. C and O. G. F. contribute equally to this work

*Corresponding author: Beiyan Nan, 306C BSBE, 3258 TAMU, College Station, TX77843

Tel.: 979-845-3487, email: bnan@tamu.edu

Abstract

The Gram-negative bacterium *Myxococcus xanthus* glides on solid surfaces. Dynamic bacterial focal adhesion complexes (bFACs) convert proton motive force from the inner membrane into mechanical propulsion on cell surface. It is unclear how the mechanical force transmits across the rigid peptidoglycan (PG) cell wall. Here we show that AgmT, a highly abundant lytic PG transglycosylase homologous to *Escherichia coli* MltG, couples bFACs to PG. Coprecipitation assay and single-particle microscopy reveal that the gliding motors fail to connect to PG and thus are unable to assemble into bFACs in the absence of an active AgmT. Heterologous expression of *E. coli* MltG restores the connection between PG and bFACs and thus rescues gliding motility in the *M. xanthus* cells that lack AgmT. Our results indicate that bFACs anchors to AgmT-modified PG to transmit mechanical across the PG cell wall.

Introduction

In natural ecosystems, the majority of bacteria attaches to surfaces[1]. Surface-associated motility is critical for many bacteria to navigate and populate their environments[2]. The Gram-negative bacterium *Myxococcus xanthus* moves on solid surfaces using two independent mechanisms: social (S-) motility and adventurous (A-) motility. S-motility, analogous to the twitching motility in *Pseudomonas* and *Neisseria*, is powered by the extension and retraction of type IV pili[3,4]. A-motility, also known as gliding motility, does not depend on conventional motility-related cell surface appendages, such as flagella or pili[2,5]. In *M. xanthus*, AglR, AglQ, and AglS form a membrane channel that functions as the gliding motor by harvesting proton motive force[6,7]. The motor unit associates with at least fourteen gliding-related proteins that reside in the cytoplasm, inner membrane, periplasm, and outer membrane[8-10].

Recently, the mechanisms for bFAC assembly and the coupling between bFACs and substrate begin to emerge[8,11,12]. In each gliding cell, two distinct populations of gliding complexes coexist: dynamic complexes move along helical paths and static complexes remain fixed relative to the substrate[11,13-15]. Motors transport incomplete gliding complexes along helical tracks but form complete, force-generating complexes at the ventral side of cells that appear fixed to the substrate (**Fig. 1**)[11,15]. Based on their functional analogy with eukaryotic focal adhesion sites, these complete gliding machineries are called bacterial focal adhesion complexes (bFACs). Despite their static appearance, bFACs are dynamic under single-molecule microscopy. Individual motors frequently display move-stall-move patterns, in which they move rapidly along helical trajectories, join a bFAC where they remain stationary briefly, then move rapidly again toward next bFAC or reverse their moving directions[13,16,17]. bFACs adhere to the gliding substrate through an outer membrane adhesin[12]. As motors transport bFACs toward

47 lagging cell poles, cells move forward but bFACs remain static relative to the gliding
48 substrate.

49 bFAC assembly can be quantified at nanometer resolution using the single-particle
50 dynamics of gliding motors[13,18]. Single particles of a fully functional, photoactivatable
51 mCherry (PAmCherry)-labeled AglR display three dynamic patterns, stationary,
52 directed motion, and diffusion[13,18]. The stationary population consists of the motors in
53 fully assembled bFACs, which do not move before photobleach. In contrast, the motors
54 moving in directed manner carry incomplete gliding complexes along helical tracks,
55 whereas the diffusing motors assemble to even less completeness[11,13,15,18]. As motors only
56 generate force in static bFACs[11], the population of nonmotile motors indicates the
57 overall status of fully assembled bFACs.

58 However, how bFACs transmit force across the peptidoglycan (PG) cell wall is
59 unclear. PG is a mesh-like single molecule of crosslinked glycan strands that surrounds
60 the entire cytoplasmic membrane. The rigidity of PG defines cell shape and protects cell
61 from osmotic lysis[19,20]. If bFACs physically penetrate PG, their transportation toward
62 lagging cell poles would tear PG and trigger cell lysis. To avoid breaching PG, an
63 updated model proposes that there are two subcomplexes in each bFAC, one on each
64 side of the PG layer. Rather than forming stable and rigid interactions, these two
65 subcomplexes only associate transiently to form a bFAC[11,21] (**Fig. 1**).

66 As motors reside in the fluid inner membrane, to transmit force to the cell surface,
67 they must push against two relatively rigid structures, one on each side of the
68 membrane, in opposite directions[21] (**Fig. 1**). MreB is a bacterial actin homolog that
69 associates with the motors and plays essential roles in gliding[2,5,6,14,18,22]. The motors could
70 push against MreB filaments in the cytoplasm, whereas PG could be the structure that

71 motors push against in the periplasm[11,21]. The interaction between the inner complex
72 and PG not only satisfies the physical requirement for force generation but also
73 supports efficient bFACs assembly. Without this interaction, once the inner subcomplex
74 disassociates from the outer one, it will quickly escape bFACs and no longer contribute
75 to force generation[21]. In this case, the fraction of time each motor generates force
76 (remains in bFACs) will be extremely low[21]. How the inner complex interacts with PG
77 remains unknown. It was speculated that gliding motors in the inner complex could
78 bind PG directly[11]. However, such binding has not been confirmed by experiments.

79 In this study, we found that AgmT, a lytic transglycosylase (LTG) for PG, is
80 essential for *M. xanthus* gliding motility. AgmT is required for maintaining PG integrity
81 under the stress from the antibiotic mecillinam. Using single-particle tracking
82 microscopy and coprecipitation assays, we found that AgmT is required for the gliding
83 motors to connect to PG and stall in bFACs. Importantly, expressing *Escherichia coli*
84 MltG heterologously rescues the connection between PG and bFACs and thus restores
85 gliding motility. Hence, the LTG activity of AgmT anchors bFAC to PG, potentially by
86 modifying PG structure. Our findings reveal the long-sought connection between PG
87 and bFAC that allows mechanic force to transmit across the PG cell wall.

88 **Results**

89 **AgmT, a putative LTG, is essential for gliding motility.** To elucidate how bFACs
90 interact with PG, we searched for potential PG-binding domains among the proteins
91 that are required for gliding motility. A previous report identified 35 gliding-related
92 genes in *M. xanthus* through transposon-mediated random mutagenesis[23]. Among these
93 genes, *agmT* (ORF K1515_04910[24]) was predicted to encode a protein with a large
94 "periplasmic solute-binding" domain[23]. After careful analysis, we found that AgmT
95 showed significant similarity to the widely conserved YceG/MltG family LTGs. About
96 70% of bacterial genomes, including firmicutes, proteobacteria, and actinobacteria,
97 encode YceG/MltG domains[25]. Especially, the putative active site, Glu223
98 (corresponding to E218 in *E. coli* MltG)[25], is conserved in AgmT (**Fig. 2A**). To confirm
99 the function of AgmT in gliding, we constructed an *agmT* in-frame deletion mutant. To
100 eliminate S-motility, we further knocked out the *pilA* gene that encodes pilin for type IV
101 pilus. In contrast to the *pilA*$^-$ cells that were still motile with gliding motility, the *ΔaglR*
102 *pilA*$^-$ cells that lack an essential component in the gliding motor, were unable to move
103 outward from the colony edge. Similarly, the *ΔagmT pilA*$^-$ cells also formed sharp colony
104 edges, indicating that they were nonmotile with gliding (**Fig. 2B**). As AgmT is a
105 putative LTG for PG, we then tested if its predicted active site, Glu223, is required for
106 gliding. Because the amino acid following Glu223 is also a glutamate (Glu224), we
107 replaced both glutamate residues with alanine (AgmT^{EAEA}) using site-directed
108 mutagenesis to alter their codons on the chromosome. *agmT*^{EAEA} *pilA*$^-$ cells were
109 nonmotile (**Fig. 2B**). Thus, the putative LTG activity of AgmT is essential for *M. xanthus*
110 gliding motility.

111 Besides *agmT*, the genome of *M. xanthus* contains 13 genes that encode putative
112 LTGs (**Table S1**). To test if these proteins also contribute to gliding, we knocked out
113 each of these 13 genes in the *pilA*$^-$ background. The resulted mutants all retained gliding

114 motility, indicating that AgmT is the only LTG that is required for *M. xanthus* gliding
115 (**Fig. S1**).

116 **AgmT is an LTG.** To determine if AgmT is an LTG, we expressed the periplasmic
117 domain (amino acids 25 – 339) of wild-type AgmT and AgmT^{EAEA} in *E. coli*. We purified
118 PG from wild-type *M. xanthus* cells, labeled it with Remazol brilliant blue (RBB), and
119 tested if the purified AgmT variants hydrolyze labeled PG *in vitro* and release the
120 dye[26,27]. Similar to lysozyme that specifically cleaves the β-1,4-glycosidic bounds in PG,
121 wild-type AgmT solubilized dye-labeled *M. xanthus* PG that absorbed light at 595 nm.
122 In contrast, the AgmT^{EAEA} variant failed to release the dye (**Fig. 3A**). Hence, AgmT
123 displays LTG activity *in vitro*.

124 Whereas AgmT does not affect growth rate (**Fig. S2**), cells that lacked AgmT or
125 expressed AgmT^{EAEA} maintained rod shape but were slightly shorter and wider than the
126 wild-type ones (**Fig. 3B**). Nevertheless, altered morphology alone does not likely
127 account for abolished gliding. In fact, a previously reported mutant that lacks all three
128 class A penicillin-binding proteins (*Δ*3) displays similarly shortened and widened
129 morphology[28], but is still motile by gliding (**Fig. S1**).

130 A recent report revealed that *Vibrio cholerae* MltG degrades un-crosslinked PG
131 turnover products and prevents their detrimental accumulation in the periplasm[29]. To
132 test if AgmT plays a similar role in *M. xanthus*, we used mecillinam to induce cell
133 envelope stress. Mecillinam is a β-lactam that induces the production of toxic, un-
134 crosslinked PG strands[30]. Rather than collapsing the rod shape, mecillinam only causes
135 bulging near the centers of wild-type *M. xanthus* cells, whereas large-scale cell lysis does
136 not occur and cell poles still maintain rod shape even after prolonged (20 h) treatment
137 (**Fig. 3C**)[28]. Thus, wild-type *M. xanthus* can largely mitigate mecillinam stress. In

138 contrast, mecillinam-treated *agmT* cells increased their width drastically, displayed
139 significant cell surface irregularity along their entire cell bodies, and lysed frequently
140 (**Fig. 3C**). Cells expressing AgmT^{EAEA} as the sole source of AgmT displayed similar, but
141 even stronger phenotypes under mecillinam stress, growing into elongated, twisted
142 filaments that formed multiple cell poles and lysed frequently (**Fig. 3C**). These results
143 confirm that similar to *V. cholerae* MltG, *M. xanthus* AgmT is important for maintaining
144 cell integrity under mecillinam stress. The different responses from *agmT* and *agmT^{EAEA}*
145 cells suggest that AgmT could interact with other PG-related enzymes and that the
146 inactive AgmT variant might still modulate PG through these enzymes. Alternatively,
147 other LTGs could partially substitute AgmT while AgmT^{EAEA} blocks these enzymes
148 from accessing un-crosslinked PG strands.

149 **AgmT is essential for bFACs assembly.** How does AgmT support gliding? We first
150 tested if AgmT regulates the function of the gliding motor. For this purpose, we
151 quantified the motor dynamics by tracking single particles of AglR, an essential
152 component of the motor. We spotted the cells that express a fully functional, photo-
153 activatable mCherry (PAmCherry)-labeled AglR[13] on 1.5% agar surface. We used a 405-
154 nm excitation laser to activate the fluorescence of a few labeled AglR particles randomly
155 in each cell and quantified their localization using a 561-nm laser at 10 Hz using single
156 particle tracking photo-activated localization microscopy (sptPALM) under highly
157 inclined and laminated optical sheet (HILO) illumination[13,18,31]. Using this setting, only a
158 thin section of each cell surface that was close to the coverslip was illuminated. To
159 analyze the data, we only chose the fluorescent particles that remained in focus for 4 -
160 12 frames (0.4 - 1.2 s). As free PAmCherry particles diffuse extremely fast in the
161 cytoplasm, entering and exiting the focal plane frequently, they usually appear as
162 blurry objects that cannot be followed at 10-Hz close to the membrane[18]. For this reason,
163 the noise from any potential degradation of AglR-PAmCherry was negligible.

164 Consistent with our previous results[13,16], 32.1% (n = 2,700) of AglR-PAmCherry particles
165 remained within one pixel (160 nm × 160 nm) before photobleach, indicating that they
166 were nonmotile. The rest 67.9% AglR-PAmCherry particles were motile, leaving
167 trajectories of various lengths (**Fig. 4A, 4B**).

168 bFAC assembly is sensitive mechanical cues. As the agar concentration increases in
169 gliding substrate, more motor molecules engage in bFACs, where they appear
170 immobile[10,15]. We exposed *aglR-PAmCherry* cells to 405-nm excitation (0.2 kW/cm^2) for 2
171 s, where most PAmCherry molecules were photoactivated and used epifluorescence to
172 display the overall localization of AglR[13,18,32]. As the agar concentration increased bFACs
173 increased significantly in size (**Fig. 4C**). Accordingly, the immobile AglR particles
174 detected by sptPALM increased from 10.7% (n = 1112) on 0.5% agar to 45.2% (n = 726)
175 on 5.0% agar surface (**Fig. 4B**). Thus, the stationary population of AglR-PAmCherry
176 particles reflects the AglR molecules in fully assembled bFACs.

177 In contrast to the cells that expressed wild-type AgmT (*agmT*$^+$), AglR particles were
178 hyper motile in the cells that lacked AgmT or expressed AgmT^{EAEA}. On 1.5% agar
179 surfaces, the immobile populations of AglR particles decreased to 10.5% (n = 2,989) and
180 11.7% (n = 1,408), respectively. Consistently, AglR-containing bFACs were not
181 detectable in these cells, even on 5% agar surfaces (**Fig. 4A-C**).

182 To test if other components in the gliding machinery also depend on AgmT to
183 assemble into bFACs, we tested the localization of AglZ, a cytoplasmic protein that is
184 commonly used for assessing bFAC assembly[11,33]. In the cells that expressed wild-type
185 AgmT, yellow fluorescent protein (YFP)-labeled AglZ formed a bright cluster at the
186 leading cell pole and multiple stationary, near-evenly spaced clusters along the cell
187 body, indicating the assembly of bFACs (**Fig. 4D**). In contrast, AglZ-YFP only formed

188 single clusters at cell poles in the cells that lacked AgmT or expressed AgmT^{EAEA} (**Fig.**
189 **4D**). Taken together, the LTG activity of AgmT is essential for bFACs assembly.

190 **AgmT does not assemble into bFACs.** We first hypothesized that AgmT itself could
191 assemble into bFACs, where it could either generate pores in PG that allow the inner
192 and outer gliding complexes interact directly or bind to PG and recruit other
193 components to bFACs through protein-protein interactions. If this is the case, AgmT
194 should localize in bFACs. To test this possibility, we labeled AgmT with PAmCherry on
195 its C-terminus and expressed the fusion protein as the sole source of AgmT using the
196 native promoter and locus of *agmT*. *agmT-PAmCherry pilA*$^{-}$ cells displayed gliding
197 motility that was indistinguishable from *pilA*$^{-}$ cells (**Fig. 2B**), indicating that the fusion
198 protein is functional. Immunoblot using an anti-mCherry antibody showed that AgmT-
199 PAmCherry accumulated in two bands that corresponded to monomers and dimers of
200 the full-length fusion protein, respectively (**Fig. 5A**). This result is consistent with the
201 structure of *E. coli* MltG that functions as homodimers (PDB: 2r1f). Importantly, AgmT-
202 PAmCherry was about 50 times more abundant than AglR-PAmCherry (**Fig. 5A**). To
203 test if AgmT itself assembles into bFACs, we first expressed AgmT-PAmCherry and
204 AglZ-YFP together using their respective loci and promoter. We exposed *agmT-*
205 *PAmCherry* cells to 405-nm excitation (0.2 kW/cm^2) for 2 s to visualize the overall
206 localization of AgmT. We found that on a 1.5% agar surface that favors gliding motility,
207 AglZ aggregated into bFACs whereas AgmT localized near evenly along cell bodies
208 without forming protein clusters (**Fig. 5B**). Thus, AgmT does not localize into bFACs.
209 These results echo the fact that despite to its abundancy, AgmT has not been identified
210 as a component in bFACs despite extensive pull-down experiments using various bFAC
211 components as baits[6,10,34].

212 We reasoned that if AgmT assembles into bFACs, AgmT and gliding motors should
213 display similar dynamic patterns. To test this possibility further, we used sptPALM to
214 track the movements of AgmT-PAmCherry single particles on 1.5 agar surfaces at 10
215 Hz. Distinct from the AglR particles of which 32.1% remained stationary, AgmT moved
216 in a diffusive manner, showing no significant immobile population. Importantly,
217 compared to the diffusion coefficients (D) of mobile AglR particles ($1.8 \times 10^{-2} \pm 3.6 \times 10^{-3}$
218 $\mu m^2/s$ (n = 1,833)), AgmT particles diffused much faster ($D = 2.9 \times 10^{-2} \pm 5.3 \times 10^{-3}$ $\mu m^2/s$
219 (n = 8,548)). Taken together, neither the localization nor dynamics of AgmT displayed
220 significant correlation with bFAC components. We thus conclude that AgmT does not
221 assemble into bFACs

222 **AgmT connects bFACs to PG through its LTG activity.** We then explored the
223 possibility that AgmT could modify PG through its LTG activity and thus generate the
224 anchor sites for certain components in bFACs. If this hypothesis is true, heterologous
225 expression of a non-native LTG could rescue gliding motility in the *ΔagmT* strain. To
226 test this hypothesis, we fused the *E. coli mltG* gene ($mltG_{Ec}$) to a vanillate-inducible
227 promoter and inserted the resulted construct to the *cuoA* locus on *M. xanthus*
228 chromosome that does not interfere gliding[35]. We subjected the *ΔagmT* and $agmT^{EAEA}$
229 cells that expressed $MltG_{Ec}$ to mecillinam (100 μg/ml) stress. Induced by 100 μM sodium
230 vanillate, $MltG_{Ec}$ restored cell morphology and integrity of the *ΔagmT* strain to the wild-
231 type level (**Fig. 3C**). This result confirmed that $MltG_{Ec}$ was expressed and enzymatically
232 active in *M. xanthus*. In contrast, $MltG_{Ec}$ failed confer mecillinam resistance to the
233 $agmT^{EAEA}$ cells (**Fig. 3C**). A potential explanation is that $AgmT^{EAEA}$ could still bind to PG
234 and thus block $MltG_{Ec}$ from accessing *M. xanthus* PG. Consistent with its activity, $MltG_{Ec}$
235 restored gliding motility in the *agmT pilA* cells but not in the $agmT^{EAEA}$ *pilA* ones (**Fig.
236 2B**). As $MltG_{Ec}$ substitutes AgmT in gliding motility, it is the LTG activity, rather than
237 specific interactions between AgmT and bFACs, that is required for gliding.

238 It is challenging to visualize how AgmT facilitates bFAC assembly through its
239 enzymatic activity *in vitro*. First, the inner complex in a bFAC spans the cytoplasm,
240 inner membrane, and periplasm and contains multiple proteins whose activities are
241 interdependent[8,10,11]. It is hence difficult to purify the entire inner complex in its
242 functional state. Second, Faure *et al*. hypothesized that AglQ and AglS in the gliding
243 motor could bind PG directly[11]. However, such binding has not been proved
244 experimentally due to the difficulty in purifying the membrane integral AglRQS
245 complex. To overcome these difficulties, we used AglR-PAmCherry to represent the
246 inner complex of bFAC and investigated how bFACs bind PG in their native
247 environment. To do so, we expressed AglR-PAmCherry in different genetic
248 backgrounds as the sole source of AglR using the native *aglR* locus and promoter. We
249 lysed these cells using sonication, subjected their lysates to centrifugation, isolated the
250 pellets that contained PG, and detected the presence of AglR-PAmCherry in these
251 pellets by immunoblots using a mCherry antibody. Eliminating AgmT and disabling its
252 active site significantly reduced the amounts of AglR in the pellets (**Fig. 5B**). Because
253 such pellets contain both the PG and membrane fractions, we further eliminated PG in
254 cell lysates using lysozyme before centrifugation and determined the amount of AglR-
255 PAmCherry in the pellets that only contained membrane fractions. Regardless the
256 presence and activity of AgmT, comparable amounts of AglR precipitated in
257 centrifugation pellets after lysozyme treatment, indicating that AgmT does not affect
258 the expression or stability of AglR (**Fig. 5B**). Thus, active AgmT facilitates the
259 association between bFACs and PG. Strikingly, the heterologous expression of $MltG_{Ec}$
260 enriched AglR-PAmCherry in the PG-containing pellets from the *ΔagmT* cells but not
261 the $agmT^{EAEA}$ ones (**Fig. 5B**). These results indicate that AgmT connects bFACs to PG
262 through its LTG activity.

263

264 **Discussion**

265 Gliding bacteria adopt a broad spectrum of nanomachineries. Compared to the trans-
266 envelope secretion system that drives gliding in *Flavobacterium johnsoniae* and
267 *Capnocytophaga gingivalis* that both contain PG, the gliding machinery of *M. xanthus*
268 appears to lack a stable structure that transverses cell envelope, especially across the PG
269 layer[2,36,37]. In order to generate mechanical force from the fluid *M. xanthus* gliding
270 machinery, the inner complex must establish solid contact with PG and push the outer
271 complex to slide[11,21]. In this work, we discovered AgmT as the long-sought factor that
272 connects bFACs to PG. Such connection not only satisfies the requirement for force
273 generation but is also essential for bFAC assembly.

274 It is rather unexpected that AgmT itself does not assemble into bFACs. Because
275 $MltG_{Ec}$ substitutes AgmT in gliding, rather than interacting with bFAC components
276 specifically, AgmT facilitates bFAC assembly through its LTG activity. A few
277 possibilities could explain the function of AgmT. First, LTGs usually break glycan
278 strands and produce unique anhydro caps on their ends[38-41]. Certain components in
279 bFACs could specifically bind to such modified glycan strands in PG and further recruit
280 other components. Second, AgmT could generate small openings all over the PG
281 meshwork that allow the inner and outer subcomplexes in bFACs to interact locally.
282 Third, AgmT could reduce the overall rigidity of *M. xanthus* PG, allow the bulky inner
283 subcomplexes to deform the PG layer, and thus establish a viscous coupling between
284 bFACs and PG[6,21].

285 Then how does AgmT, a protein localizes diffusively, facilitate bFAC assembly into
286 near-evenly spaced foci? The actin homolog MreB is the only protein in bFACs that
287 displays quasiperiodic localization independent of other components[18,22]. *M. xanthus*
288 MreB assembles into bFACs and positions the latter near evenly along the cell
289 body[6,13,18,22,42]. MreB filaments change their orientation in accordance with local

290 membrane curvatures and could hence respond to mechanical cues[43-46]. Strikingly, *M.*
291 *xanthus* does assemble bFACs in response to substrate hardness (**Fig. 4C**) and
292 assembled bFACs could distort cell envelope, generating undulations on cell
293 surface[6,10,13,47,48]. Taken together, whereas AgmT potentially modifies the entire PG layer,
294 it is still the quasiperiodic MreB filaments that determine the loci for bFAC assembly in
295 response to the mechanical cues from the gliding substrate.

296 Most bacteria encode multiple LTGs that function in PG growth, remodeling, and
297 recycling. Trans-envelope structures often require highly specialized LTGs to penetrate
298 PG[49]. This work provides an example that macro bacterial machineries domesticate non-
299 specialized LTGs for specialized functions. Other examples include MltD in the
300 *Helicobacter pylori* flagellum and MltE in the *E. coli* type VI secretion system[50,51]. Both *M.*
301 *xanthus* AgmT and *E. col*i MltG belong to the YceG family, which is the first identified
302 LTG family that is conserved in both Gram-negative and positive bacteria[39]. LTGs in
303 this family localize to the inner membrane and feature periplasmic transglycosylase
304 domains[39]. Due to their unique localization, the YceG family LTGs are important for
305 determining the length of nascent glycan strands and for degrading the toxic un-
306 crosslinked strands from futile PG synthesis[29,52]. Due to the wide distribution of YceG
307 family LTGs, it is challenging to study how the unique *M. xanthus* gliding machinery
308 adopts AgmT in evolution. Nevertheless, the fact that AgmT is the only *M. xanthus* LTG
309 that belongs to this family (**Table S2**) could partially explain why it is the only LTG that
310 has been adopted by the gliding machinery. It will be interesting to investigate if other
311 LTGs, once anchored to the inner membrane, could also facilitate bFAC assembly.

312 **Methods**

313 **Strains and growth conditions**

314 *M. xanthus* strains used in this study are listed in **Table S2**. Vegetative *M. xanthus* cells
315 were grown in liquid CYE medium (10 mM MOPS pH 7.6, 1% (w/v) Bacto™ casitone (BD
316 Biosciences), 0.5% yeast extract and 8 mM $MgSO_4$) at 32 °C, in 125-ml flasks with rigorous
317 shaking, or on CYE plates that contains 1.5% agar. All genetic modifications on *M. xanthus*
318 were made on chromosome. Deletion and insertion mutants were constructed by
319 electroporating *M. xanthus* cells with 4 μg of plasmid DNA. Transformed cells were
320 plated on CYE plates supplemented with 100 μg/ml sodium kanamycin sulfate and 10
321 μg/ml tetracycline hydrochloride when needed. AgmT and $AgmT^{EAEA}$ were labeled with
322 PAmCherry at their C-termini by fusing their gene to a DNA sequence that encodes
323 PAmCherry through a KESGSVSSEQLAQFRSLD
324 (AAGGAGTCCGGCTCCGTGTCCTCCGAGCAGCTGGCCCAGTTCCGCTCCCTGGA
325 C) linker. All constructs were confirmed by PCR and DNA sequencing.

326 **Immunoblotting**

327 The expression and stability of PAmCherry-labeled proteins were determined by
328 immunoblotting using an anti-mCherry antibody (Rockland Immunochemicals, Inc., Lot
329 46705) and a goat anti-Rabbit IgG (H+L) secondary antibody, HRP (Thermo Fisher
330 Scientific, catalog # 31460). MreB was detected using an anti-MreB serum[22] and the same
331 secondary antibody. The blots were developed with Pierce™ ECL Western Blotting
332 Substrate (Thermo Fisher Scientific REF 32109) and MINI-MED 90 processor (AFP
333 Manufacturing).

334 **Gliding assay**

335 Cells at 4×10^9 colony formation units (cfu)/ml were spotted on CYE plates (5 μl/spot)
336 containing 1.5% agar, incubated at 32 °C for 48 h. Colony edges were photographed

337 using a Nikon Eclipse™ 600 microscope with a 10× 0.30 NA objective and an OMAX™
338 A3590U camera.

339 **Protein expression and purification**

340 DNA sequences encoding amino acids 25 – 339 of AgmT and AgmT^{EAEA} were amplified
341 by polymerase chain reaction (PCR) and inserted into the pET28a vector (Novogen)
342 between the restriction sites of *Eco*RI and *Hind*III. The resulted plasmids were
343 transformed into *E. coli* strain BL21(DE3). Transformed cells were cultured in 20 ml LB
344 (Luria-Bertani) broth at 37 °C overnight and used to inoculate 1 L LB medium
345 supplemented with 1.0% glucose. Protein expression was induced by 0.1 mM IPTG
346 (isopropyl-h-d-thiogalactopyranoside) when the culture reached an OD_{600} of 0.8.
347 Cultivation was continued at 16 °C for 10 h before the cells were harvested by
348 centrifugation at 6,000 × g for 20 min. Proteins were purified using the NGC™
349 Chromatography System (BIO-RAD) and a 5-ml HisTrap™ (Cytiva)[17,53]. Purified
350 proteins were concentrated using Amicon™ Ultra centrifugal filter units (Millipore
351 Sigma) with a molecular cutoff of 10 kDa and stored at -80 °C.

352 **RBB assay**

353 PG was purified following the published protocol[28,54]. In brief, *M. xanthus* cells were
354 grown until mid-stationary phase and harvested by centrifugation (6,000 × g, 20 min, 25
355 °C). Supernatant was discarded and the pellet was resuspended and boiled in 1× PBS
356 with 5% SDS for 2 h. SDS was removed by repetitive wash with MilliQ water and
357 centrifugation (21,000 × g, 10 min, 25 °C). Purified PG from 100 ml culture was
358 suspended into 1 ml 1× PBS and stored at -20 °C. RBB labelling of PG was performed
359 essentially as previously described[26,27]. Purified sacculi were incubated with 20 mM RBB
360 in 0.25 M NaOH overnight at 37 °C. Reactions were neutralized by adding equal
361 volumes of 0.25 M HCl and RBB-labeled PG was collected by centrifugation at 21,000 ×

362 g for 15 min. Pellets were washed repeatedly with MilliQ water until the supernatants
363 became colorless. RBB-labelled sacculi were incubated with purified AgmT and
364 $AgmT^{EAEA}$ (1 mg/ml) at 25 °C for 12 h. lysozyme (1 mg/ml) was used as a positive
365 control. Dye release was quantified by the absorption at 595 nm from the supernatants
366 after centrifugation (21,000 × g, 10 min, 25 °C).

367 **PG binding assay**

368 *M. xanthus* cells expressing AglR-PAmCherry were grown in liquid CYE to OD_{600} ~1,
369 harvested by centrifugation (6,000 × g, 20 min, 25 °C), washed by 1× PBS, and
370 resuspended into 1× PBS to OD_{600} 6. Cells (1 ml) were lysed using a Cole-Parmer 4710
371 Ultrasonic Homogenizer (40% output). Unbroken cells and large debris were eliminated
372 by centrifugation (6,000 × g, 10 min, 25 °C). Supernatants were subjected to
373 centrifugation at 21,000 × g for 15 min. Pellets that contains the PG and membrane
374 fractions were resuspended to 1 ml in 1× PBS. To collect the pellets that do not contain
375 PG, supernatants from sonication lysates were incubated with 5 mg/ml lysozyme at 25
376 °C for 5 h before centrifugation. Resuspended pellets (5 μl each) were mixed with equal
377 volumes of 2× loading buffer and applied to SDS PAGE and immunoblotting.

378 **Microscopy Analysis**

379 For all imaging experiments, 5 μl cells were spotted on an agarose pad. For the
380 treatments with inhibitors, inhibitors were added into both the cell suspension and
381 agarose pads. The length and width of cells were determined from differential
382 interference contrast (DIC) images using a MATLAB (MathWorks) script[18,28,55]. DIC and
383 fluorescence images of cells were captured using a Hamamatsu ImagEM X2™ EM-CCD
384 camera C9100-23B (effective pixel size 160 nm) on an inverted Nikon Eclipse-Ti™
385 microscope with a 100× 1.49 NA TIRF objective. For sptPALM, *M. xanthus* cells were
386 grown in CYE to 4 ×10^8 cfu/ml and PAmCherry was activated using a 405-nm laser (0.3

387 kW/cm^2), excited and imaged using a 561-nm laser (0.2 kW/cm^2). Images were acquired
388 at 10 Hz. For each sptPALM experiment, single PAmCherry particles were localized in
389 at least 100 individual cells from three biological replicates. sptPALM data were
390 analyzed using a MATLAB (MathWorks) script[18,28,55]. Briefly, cells were identified using
391 differential interference contrast images. Single PAmCherry particles inside cells were
392 fit by a symmetric 2D Gaussian function, whose center was assumed to be the particle's
393 position[18]. Particles that explored areas smaller than 160 nm × 160 nm (within one pixel)
394 in 0.4 - 1.2 s were considered immobile. Sample trajectories were generated using the
395 TrackMate[56] plugin in the ImageJ suite (https://imagej.net).

396 ## References

397 1 Laventie, B. J. & Jenal, U. Surface Sensing and Adaptation in Bacteria. *Annu Rev Microbiol* **74**, 735-
398 760 (2020). https://doi.org:10.1146/annurev-micro-012120-063427
399 2 Nan, B. & Zusman, D. R. Novel mechanisms power bacterial gliding motility. *Mol Microbiol* **101**,
400 186-193 (2016). https://doi.org:10.1111/mmi.13389
401 3 Chang, Y. W. *et al.* Architecture of the type IVa pilus machine. *Science* **351**, aad2001 (2016).
402 https://doi.org:10.1126/science.aad2001
403 4 Wu, S. S. & Kaiser, D. Genetic and functional evidence that Type IV pili are required for social
404 gliding motility in *Myxococcus xanthus*. *Mol Microbiol* **18**, 547-558 (1995).
405 5 Nan, B. & Zusman, D. R. Uncovering the mystery of gliding motility in the myxobacteria. *Annu Rev*
406 *Genet* **45**, 21-39 (2011). https://doi.org:10.1146/annurev-genet-110410-132547
407 6 Nan, B. *et al.* Myxobacteria gliding motility requires cytoskeleton rotation powered by proton
408 motive force. *Proc Natl Acad Sci U S A* **108**, 2498-2503 (2011).
409 https://doi.org:10.1073/pnas.1018556108
410 7 Sun, M., Wartel, M., Cascales, E., Shaevitz, J. W. & Mignot, T. Motor-driven intracellular transport
411 powers bacterial gliding motility. *Proc Natl Acad Sci U S A* **108**, 7559-7564 (2011).
412 https://doi.org:1101101108 [pii] 10.1073/pnas.1101101108
413 8 Jakobczak, B., Keilberg, D., Wuichet, K. & Sogaard-Andersen, L. Contact- and Protein Transfer-
414 Dependent Stimulation of Assembly of the Gliding Motility Machinery in *Myxococcus xanthus*.
415 *PLoS Genet* **11**, e1005341 (2015). https://doi.org:10.1371/journal.pgen.1005341
416 9 Luciano, J. *et al.* Emergence and modular evolution of a novel motility machinery in bacteria. *PLoS*
417 *Genet* **7**, e1002268 (2011). https://doi.org:10.1371/journal.pgen.1002268
418 10 Nan, B., Mauriello, E. M., Sun, I. H., Wong, A. & Zusman, D. R. A multi-protein complex from
419 *Myxococcus xanthus* required for bacterial gliding motility. *Mol Microbiol* **76**, 1539-1554 (2010).
420 https://doi.org:10.1111/j.1365-2958.2010.07184.x
421 11 Faure, L. M. *et al.* The mechanism of force transmission at bacterial focal adhesion complexes.
422 *Nature* **539**, 530-535 (2016). https://doi.org:10.1038/nature20121
423 12 Islam, S. T. *et al.* Unmasking of the von Willebrand A-domain surface adhesin CglB at bacterial
424 focal adhesions mediates myxobacterial gliding motility. *Sci Adv* **9**, eabq0619 (2023).
425 https://doi.org:10.1126/sciadv.abq0619
426 13 Nan, B. *et al.* Flagella stator homologs function as motors for myxobacterial gliding motility by
427 moving in helical trajectories. *Proc Natl Acad Sci U S A* **110**, E1508-1513 (2013).
428 https://doi.org:10.1073/pnas.1219982110
429 14 Nan, B., McBride, M. J., Chen, J., Zusman, D. R. & Oster, G. Bacteria that glide with helical tracks.
430 *Curr Biol* **24**, R169-R173 (2014). https://doi.org:10.1016/j.cub.2013.12.034
431 15 Nan, B. Bacterial Gliding Motility: Rolling Out a Consensus Model. *Curr Biol* **27**, R154-R156 (2017).
432 https://doi.org:10.1016/j.cub.2016.12.035
433 16 Nan, B. *et al.* The polarity of myxobacterial gliding is regulated by direct interactions between the
434 gliding motors and the Ras homolog MglA. *Proc Natl Acad Sci U S A* **112**, E186-193 (2015).
435 https://doi.org:10.1073/pnas.1421073112
436 17 Pogue, C. B., Zhou, T. & Nan, B. PlpA, a PilZ-like protein, regulates directed motility of the
437 bacterium *Myxococcus xanthus*. *Mol Microbiol* **107**, 214-228 (2018).
438 https://doi.org:10.1111/mmi.13878
439 18 Fu, G. *et al.* MotAB-like machinery drives the movement of MreB filaments during bacterial gliding
440 motility. *Proc Natl Acad Sci U S A* **115**, 2484-2489 (2018).
441 https://doi.org:10.1073/pnas.1716441115

19 Rohs, P. D. A. & Bernhardt, T. G. Growth and Division of the Peptidoglycan Matrix. *Annu Rev Microbiol* **75**, 315-336 (2021). https://doi.org:10.1146/annurev-micro-020518-120056

20 Garner, E. C. Toward a Mechanistic Understanding of Bacterial Rod Shape Formation and Regulation. *Annu Rev Cell Dev Biol* **37**, 1-21 (2021). https://doi.org:10.1146/annurev-cellbio-010521-010834

21 Chen, J. & Nan, B. Flagellar Motor Transformed: Biophysical Perspectives of the *Myxococcus xanthus* Gliding Mechanism. *Front Microbiol* **13**, 891694 (2022). https://doi.org:10.3389/fmicb.2022.891694

22 Mauriello, E. M. *et al.* Bacterial motility complexes require the actin-like protein, MreB and the Ras homologue, MglA. *Embo J* **29**, 315-326 (2010). https://doi.org:10.1038/emboj.2009.356

23 Youderian, P., Burke, N., White, D. J. & Hartzell, P. L. Identification of genes required for adventurous gliding motility in *Myxococcus xanthus* with the transposable element mariner. *Mol Microbiol* **49**, 555-570 (2003).

24 Aramayo, R. & Nan, B. *De Novo* Assembly and Annotation of the Complete Genome Sequence of *Myxococcus xanthus* DZ2. *Microbiol Resour Announc*, e0107421 (2022). https://doi.org:10.1128/mra.01074-21

25 Yunck, R., Cho, H. & Bernhardt, T. G. Identification of MltG as a potential terminase for peptidoglycan polymerization in bacteria. *Mol Microbiol* **99**, 700-718 (2016). https://doi.org:10.1111/mmi.13258

26 Uehara, T., Parzych, K. R., Dinh, T. & Bernhardt, T. G. Daughter cell separation is controlled by cytokinetic ring-activated cell wall hydrolysis. *EMBO J* **29**, 1412-1422 (2010). https://doi.org:10.1038/emboj.2010.36

27 Jorgenson, M. A., Chen, Y., Yahashiri, A., Popham, D. L. & Weiss, D. S. The bacterial septal ring protein RlpA is a lytic transglycosylase that contributes to rod shape and daughter cell separation in *Pseudomonas aeruginosa*. *Mol Microbiol* **93**, 113-128 (2014). https://doi.org:10.1111/mmi.12643

28 Zhang, H., Venkatesan, S., Ng, E. & Nan, B. Coordinated peptidoglycan synthases and hydrolases stabilize the bacterial cell wall. *Nature communications* **14**, 5357 (2023). https://doi.org:10.1038/s41467-023-41082-3

29 Weaver, A. I. *et al.* Lytic transglycosylases mitigate periplasmic crowding by degrading soluble cell wall turnover products. *Elife* **11** (2022). https://doi.org:10.7554/eLife.73178

30 Cho, H., Uehara, T. & Bernhardt, T. G. Beta-lactam antibiotics induce a lethal malfunctioning of the bacterial cell wall synthesis machinery. *Cell* **159**, 1300-1311 (2014). https://doi.org:10.1016/j.cell.2014.11.017

31 Tokunaga, M., Imamoto, N. & Sakata-Sogawa, K. Highly inclined thin illumination enables clear single-molecule imaging in cells. *Nat Methods* **5**, 159-161 (2008). https://doi.org:10.1038/nmeth1171

32 Zhang, H. *et al.* Establishing rod shape from spherical, peptidoglycan-deficient bacterial spores. *Proc Natl Acad Sci U S A* **117**, 14444-14452 (2020). https://doi.org:10.1073/pnas.2001384117

33 Mignot, T., Shaevitz, J. W., Hartzell, P. L. & Zusman, D. R. Evidence that focal adhesion complexes power bacterial gliding motility. *Science* **315**, 853-856 (2007).

34 Jolivet, N. Y. *et al.* Integrin-like adhesin CglD confers traction and stabilizes bacterial focal adhesions involved in myxobacterial gliding motility. *bioRxiv*, 2023.2010.2019.562135 (2023). https://doi.org:10.1101/2023.10.19.562135

35 Iniesta, A. A., Garcia-Heras, F., Abellon-Ruiz, J., Gallego-Garcia, A. & Elias-Arnanz, M. Two systems for conditional gene expression in *Myxococcus xanthus* inducible by isopropyl-beta-D-thiogalactopyranoside or vanillate. *J Bacteriol* **194**, 5875-5885 (2012). https://doi.org:10.1128/JB.01110-12

36 James, R. H. *et al.* Structure and mechanism of the proton-driven motor that powers type 9 secretion and gliding motility. *Nature Microbiology* **6**, 221-+ (2021). https://doi.org:10.1038/s41564-020-00823-6

37 Shrivastava, A. *et al.* Cargo transport shapes the spatial organization of a microbial community. *Proc Natl Acad Sci U S A* **115**, 8633-8638 (2018). https://doi.org:10.1073/pnas.1808966115

38 Williams, A. H. *et al.* A step-by-step in crystallo guide to bond cleavage and 1,6-anhydro-sugar product synthesis by a peptidoglycan-degrading lytic transglycosylase. *J Biol Chem* **293**, 6000-6010 (2018). https://doi.org:10.1074/jbc.RA117.001095

39 Dik, D. A., Marous, D. R., Fisher, J. F. & Mobashery, S. Lytic transglycosylases: concinnity in concision of the bacterial cell wall. *Crit Rev Biochem Mol Biol* **52**, 503-542 (2017). https://doi.org:10.1080/10409238.2017.1337705

40 Holtje, J. V., Mirelman, D., Sharon, N. & Schwarz, U. Novel type of murein transglycosylase in *Escherichia coli*. *J Bacteriol* **124**, 1067-1076 (1975). https://doi.org:10.1128/jb.124.3.1067-1076.1975

41 van Heijenoort, J. Peptidoglycan hydrolases of *Escherichia coli*. *Microbiol Mol Biol Rev* **75**, 636-663 (2011). https://doi.org:10.1128/MMBR.00022-11

42 Treuner-Lange, A. *et al.* The small G-protein MglA connects to the MreB actin cytoskeleton at bacterial focal adhesions. *J Cell Biol* **210**, 243-256 (2015). https://doi.org:10.1083/jcb.201412047

43 Hussain, S. *et al.* MreB filaments align along greatest principal membrane curvature to orient cell wall synthesis. *Elife* **7** (2018). https://doi.org:10.7554/eLife.32471

44 Wong, F., Garner, E. C. & Amir, A. Mechanics and dynamics of translocating MreB filaments on curved membranes. *Elife* **8** (2019). https://doi.org:10.7554/eLife.40472

45 Ursell, T. S. *et al.* Rod-like bacterial shape is maintained by feedback between cell curvature and cytoskeletal localization. *Proc Natl Acad Sci U S A* **111**, E1025-1034 (2014). https://doi.org:10.1073/pnas.1317174111

46 Bratton, B. P., Shaevitz, J. W., Gitai, Z. & Morgenstein, R. M. MreB polymers and curvature localization are enhanced by RodZ and predict *E. coli*'s cylindrical uniformity. *Nature communications* **9**, 2797 (2018). https://doi.org:10.1038/s41467-018-05186-5

47 Tchoufag, J., Ghosh, P., Pogue, C. B., Nan, B. & Mandadapu, K. K. Mechanisms for bacterial gliding motility on soft substrates. *Proc Natl Acad Sci U S A* **116**, 25087-25096 (2019). https://doi.org:10.1073/pnas.1914678116

48 Chen, Y., Topo, E. J., Nan, B. & Chen, J. Mathematical modeling of mechanosensitive reversal control in *Myxococcus xanthus*. *Front Microbiol* **14**, 1294631 (2023). https://doi.org:10.3389/fmicb.2023.1294631

49 Burkinshaw, B. J. *et al.* Structural analysis of a specialized type III secretion system peptidoglycan-cleaving enzyme. *J Biol Chem* **290**, 10406-10417 (2015). https://doi.org:10.1074/jbc.M115.639013

50 Roure, S. *et al.* Peptidoglycan maturation enzymes affect flagellar functionality in bacteria. *Mol Microbiol* **86**, 845-856 (2012). https://doi.org:10.1111/mmi.12019

51 Santin, Y. G. & Cascales, E. Domestication of a housekeeping transglycosylase for assembly of a Type VI secretion system. *EMBO Rep* **18**, 138-149 (2017). https://doi.org:10.15252/embr.201643206

52 Bohrhunter, J. L., Rohs, P. D. A., Torres, G., Yunck, R. & Bernhardt, T. G. MltG activity antagonizes cell wall synthesis by both types of peptidoglycan polymerases in *Escherichia coli*. *Mol Microbiol* **115**, 1170-1180 (2021). https://doi.org:10.1111/mmi.14660

53 Nan, B. *et al.* Purification and preliminary X-ray crystallographic analysis of the ligand-binding domain of *Sinorhizobium meliloti* DctB. *Biochim Biophys Acta* **1764**, 839-841 (2006). https://doi.org:10.1016/j.bbapap.2005.10.023

538 54 Alvarez, L., Hernandez, S. B., de Pedro, M. A. & Cava, F. Ultra-Sensitive, High-Resolution Liquid
539 Chromatography Methods for the High-Throughput Quantitative Analysis of Bacterial Cell Wall
540 Chemistry and Structure. *Methods Mol Biol* **1440**, 11-27 (2016). https://doi.org:10.1007/978-1-
541 4939-3676-2_2
542 55 Zhang, H., Venkatesan, S., Ng, E. & Nan, B. Coordinated peptidoglycan synthases and hydrolases
543 stabilize the bacterial cell wall. *GitHub* (2023). https://doi.org:10.5281/zenodo.8234126
544 56 Ershov, D. *et al.* TrackMate 7: integrating state-of-the-art segmentation algorithms into tracking
545 pipelines. *Nat Methods* **19**, 829-832 (2022). https://doi.org:10.1038/s41592-022-01507-1

546

547 ## Figure Legends

548 **Fig. 1. Stationary bFACs drive *M. xanthus* gliding.** Motors carrying incomplete gliding
549 complexes either diffuse or move rapidly along helical paths but do not generate propulsion.
550 Motors stall and become nearly static relative to the substrate when they assemble into
551 complete bFACs with other motor-associated proteins at the ventral side of the cell. Stalled
552 motors push MreB and bFACs in opposite directions and thus exert force against outer
553 membrane adhesins. Overall, as motors transport bFACs toward lagging cell poles, cells move
554 forward but bFACs remain static relative to the substrate. IM, inner membrane; OM, outer
555 membrane.

556 **Fig. 2. AgmT, a putative lytic transglycosylase, is required *for M. xanthus* gliding. A)**
557 AgmT shows significant similarity to a widely conserved PG transglycosylase in YceG/MltG
558 family. The conserved glutamine residue is marked by an asterisk. M_xant, *M. xanthus*; E_coli,
559 *E. coli*; M_tube, *Mycobacterium tuberculosis*; S_coel, *Streptomyces coelicolor*; A_calc,
560 *Acinetobacter calcoaceticus*; X_albi, *Xanthomonas albilineans*; N_meni, *Neisseria*
561 *menningitidis*; R_prow, *Rickettsia prowazekii*; T_aqua, *Thermus aquaticus*. **B)** AgmT is required
562 for *M. xanthus* gliding. Colony edges were imaged after incubating cells on 1.5% agar surface
563 for 24 h. Deleting or Disabling the active site of AgmT abolishes gliding but fusing an
564 PAmCherry (PAmCh) to its C-terminus does not. Heterologous Expression of *E. coli* MltG
565 restores gliding of *⊿agmT* cells but not the cells that express $AgmT^{EAEA}$.

566 **Fig. 3. AgmT regulates cell morphology and integrity under antibiotic stress. A)** Purified
567 AgmT solubilizes dye-labeled PG sacculi, but $AgmT^{EAEA}$ does not. Lysozyme serves as a
568 positive control. Absorption at 595 nm was measured after 18 h incubation at 25 °C. Data are
569 presented as mean values ± SD from three replicates. **B)** AgmT regulates cell morphology.
570 Compared to wild-type cells, cells that lack AgmT and express $AgmT^{EAEA}$ are significantly
571 shorter and wider. Heterologous expression of *E. coli* MltG partially restores cell length but not
572 cell width in *agmT* and $agmT^{EAEA}$ backgrounds. Asterisks, 200 μM sodium vanillate added. *p*
573 values were calculated using a one-way ANOVA test between two unweighted, independent
574 samples. Whiskers indicate the 25th - 75th percentiles and red dots the median. The total number
575 of cells analyzed is shown on top of each plot. **C)** AgmT regulates cell morphology and integrity
576 under mecillinam stress (100 μg/ml). Expressing *E. coli* MltG by a vanillate-inducible promoter
577 (P_{van}) restores resistance against mecillinam in *agmT* cells but not in the cells that express
578 $AgmT^{EAEA}$. van,. Arrows point to newly lysed cells. Scale bars, 5 μm.

579 **Fig. 4. AgmT and its LTG activity are essential for bFAC assembly. A)** Overall distribution
580 of AglR-PAmCherry particles on 1.5% agar surface is displayed using the composite of 100
581 consecutive frames. Single-particle trajectories of AglR-PAmCherry were generated from the
582 same frames. Individual trajectories are distinguished by colors. Deleting *agmT* or disabling the
583 transglycosylase activity of AgmT ($AgmT^{EAEA}$) decrease the stationary population of AglR
584 particles. **B)** The stationary population of AglR-PAmCherry particles, which reflects the AglR
585 molecules in bFACs, changes in response to substrate hardness (controlled by agar
586 concentration) and the presence and function of AgmT. The total number of particles analyzed
587 is shown on top of each plot. **C)** AglR fails to assemble into bFACs in the absence of active
588 AgmT, even on 5.0% agar surfaces. **D)** AgmT and its LTG activity also support the assembly of
589 AglZ into bFACs. White arrows point to bFACs. Scale bars, 5 μm.

590 **Fig. 5. AgmT does not assemble into bFACs but connects bFACs to PG. A)**
591 Immunoblotting using *M. xanthus* cell lysates and an anti-mCherry antibody shows that
592 PAmCherry-labeled AgmT and $AgmT^{EAEA}$ accumulate as full-length proteins. AgmT is
593 significantly more abundant than the motor protein AglR. The bacterial actin homolog MreB
594 visualized using an MreB antibody is shown as a loading control. **B)** AgmT does not aggregate
595 into bFACs. **C)** The LTG activity of AgmT is required for connecting bFACs to PG and
596 expressing the *E. coli* LTG MltG ($MltG_{Ec}$) restores PG binding by bFACs in cells that lack AgmT
597 but not in the ones that express an inactive AgmT variant ($AgmT^{EAEA}$). AglR-PAmCherry was
598 detected using an anti-mCherry antibody to mark the presence of bFACs that co-precipitate with
599 PG-containing (lysozyme-) pellets. Lysates from the cells that express AglR-PAmCherry in
600 different genetic backgrounds were pelleted by centrifugation in the presence and absence of
601 lysozyme.

Acknowledgements

This work is supported by the National Institute of Health R01GM129000 to B. N.. C. R. C. is supported in the 2023 – 2024 academic year by a National Institute of Health Diverse Predoctoral Training in Genetics grant T32GM135115 awarded to the Genetics and Genomics Interdisciplinary Program at Texas A&M University.

Author Contributions

C. R. C., O. G. F., and B. N. designed the study, performed experiments and data analysis, and wrote the manuscript. All authors read and approved the manuscript.

Competing Interests The authors declare no competing interests.

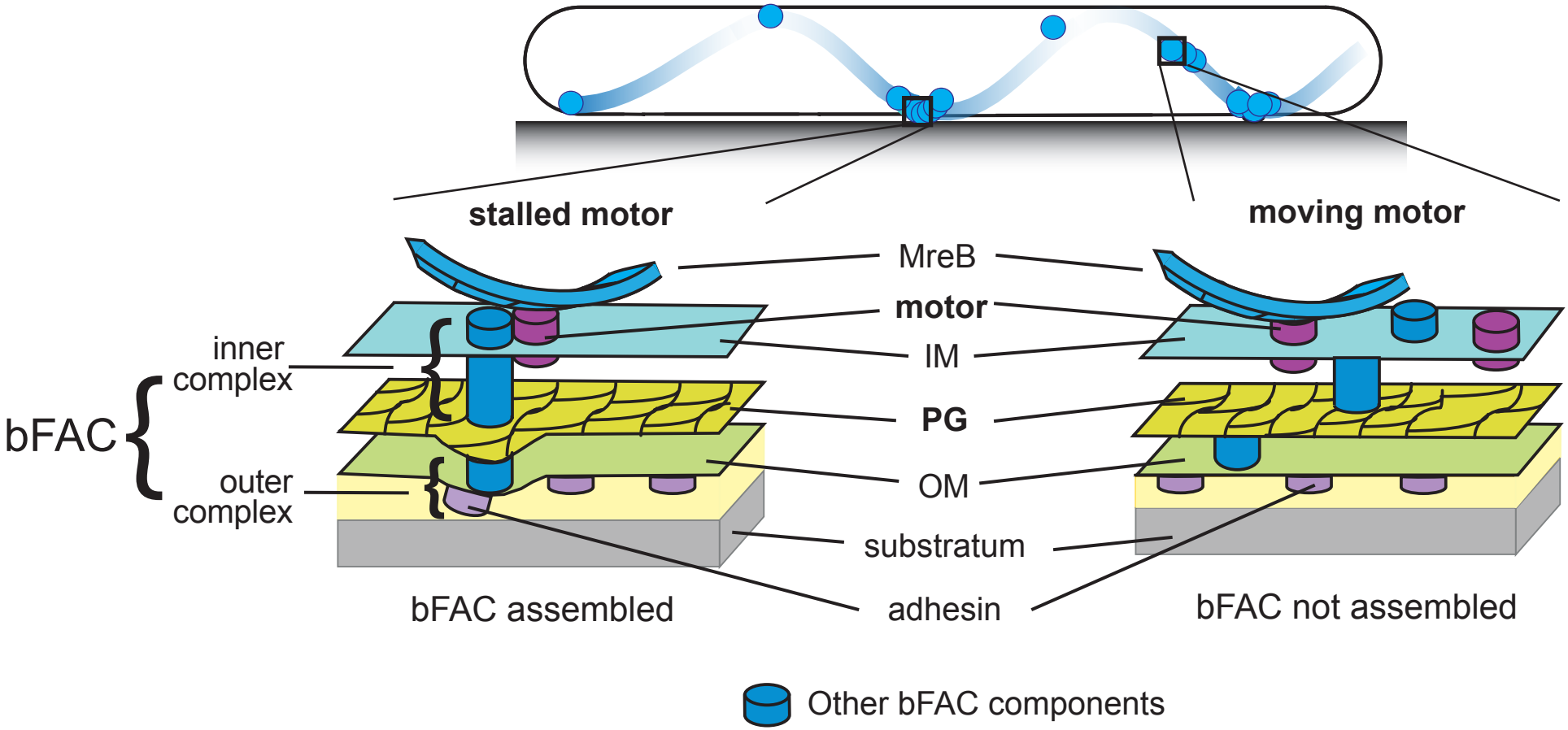
stalled motor
moving motor
MreB
motor
IM
PG
OM
substratum
adhesin
inner complex
bFAC
outer complex
bFAC assembled
bFAC not assembled
Other bFAC components

A

```
                                                                                                                                  *
M_xant  163 EGYLYPETYGVIPGKFDVEALIQRQLDAFAQRFFAPNRDTI-TKSGRTLHEVVVMASMLEREEPLPDQRPLVAGILWKRV
E_coli   88 EGWFWPDTWXYTANTTDVALLK-RAHKKXVKAVDSAWEGRADGLPYKDKNQLVTXASIIEKETAVASERDQVASVFINRL
M_tube  237 EGLIAPGTFNIDPSASAETILATLISAGAVEYMKSGLVDTAKSLGL-SPYDILVVASLVQQEAN-TQDFPKVARVIYNRL
S_coel  397 EGFLYPSSYSAAKGQKPADVLKQMVARANEQYEKIGLEQKAEGLGLEGPWELLTAASLVQAEGKTHEDFRKMAEVIYNRL
A_calc  100 EGLFAPNTYFFAKGETDKKILT-DLYHRQMKALDAAWANRAPNLPYKDKYEALIMASIVEKETSLDSELTQVSGVFVRRL
X_albi   95 EGRFLPETYLYQRGDSDLDLLR-RAHKAMDKALADAWDSRAAGLLLSSPEQALILASIVEKETALAAERPQIAGVFVRRL
N_meni  153 EGQFFPDSYEIDAGGSDLRIYQ-TAYKAMQRRLNEAWESRQDGLPYKNPYEMLIMASLIEKETGHEADRDHVASVFVNRL
R_prow   85 EGFLMPSTYFFSYGDQKDRIID-QMRNLMSTNLDEVMKYLSPDSPLKTRIDVLTLASIIEKEAGSNEEKPIIAAVFINRL
T_aqua  126 EGYLFPATYTFDLLATPEEVVR-AMLRRFEAELTPPVRQLLEERNL-SVHAWVTLASIVQVEAGSEAEMPKIAGVFLNRL
```

B

pilA

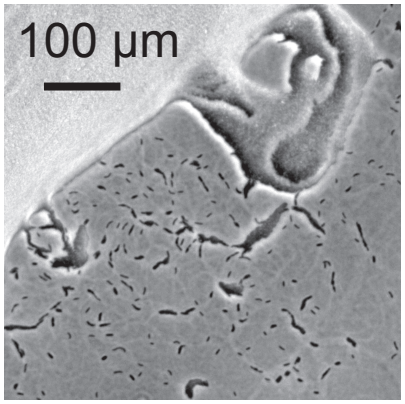

aglR pilA

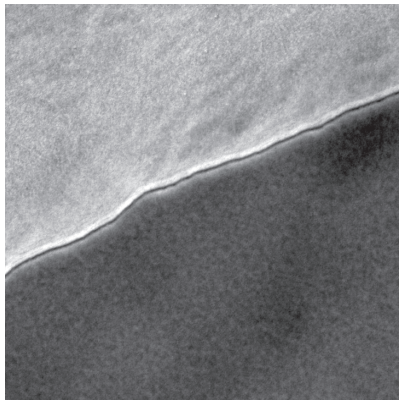

agmT pilA

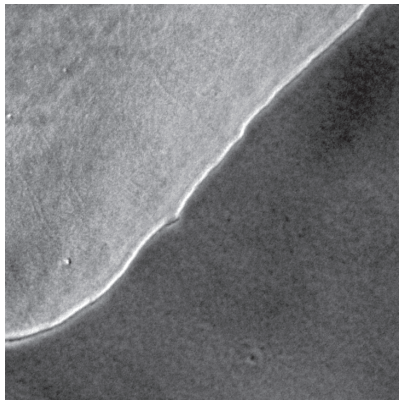

agmT^{EAEA} *pilA*

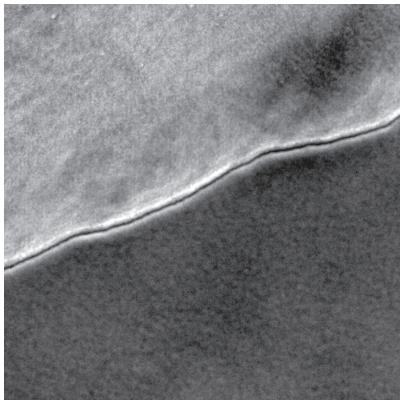

agmT-PAmCh pilA

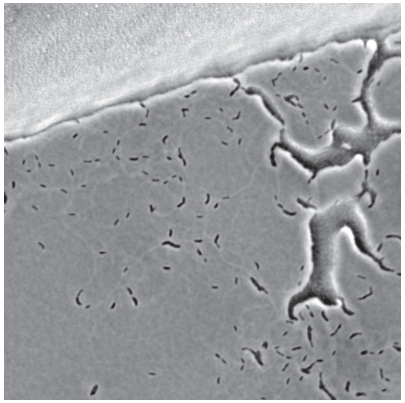

agmT pilA P_{van}*-vector*

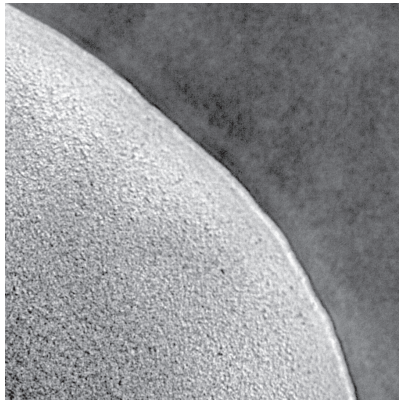

agmT pilA P_{van}*-mltG*$_{Ec}$

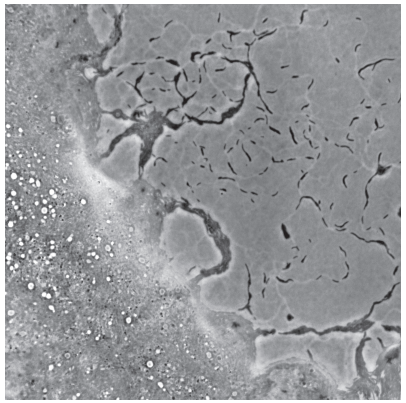

agmT^{EAEA} *pilA* P_{van}*-mltG*$_{Ec}$

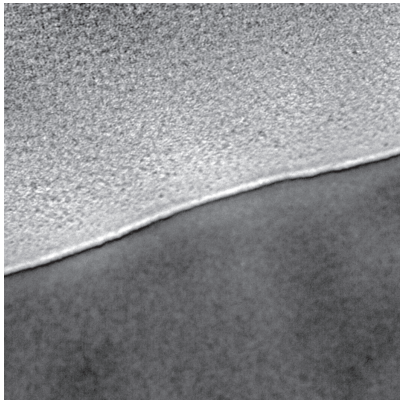

+ 200 µM Na vanillate

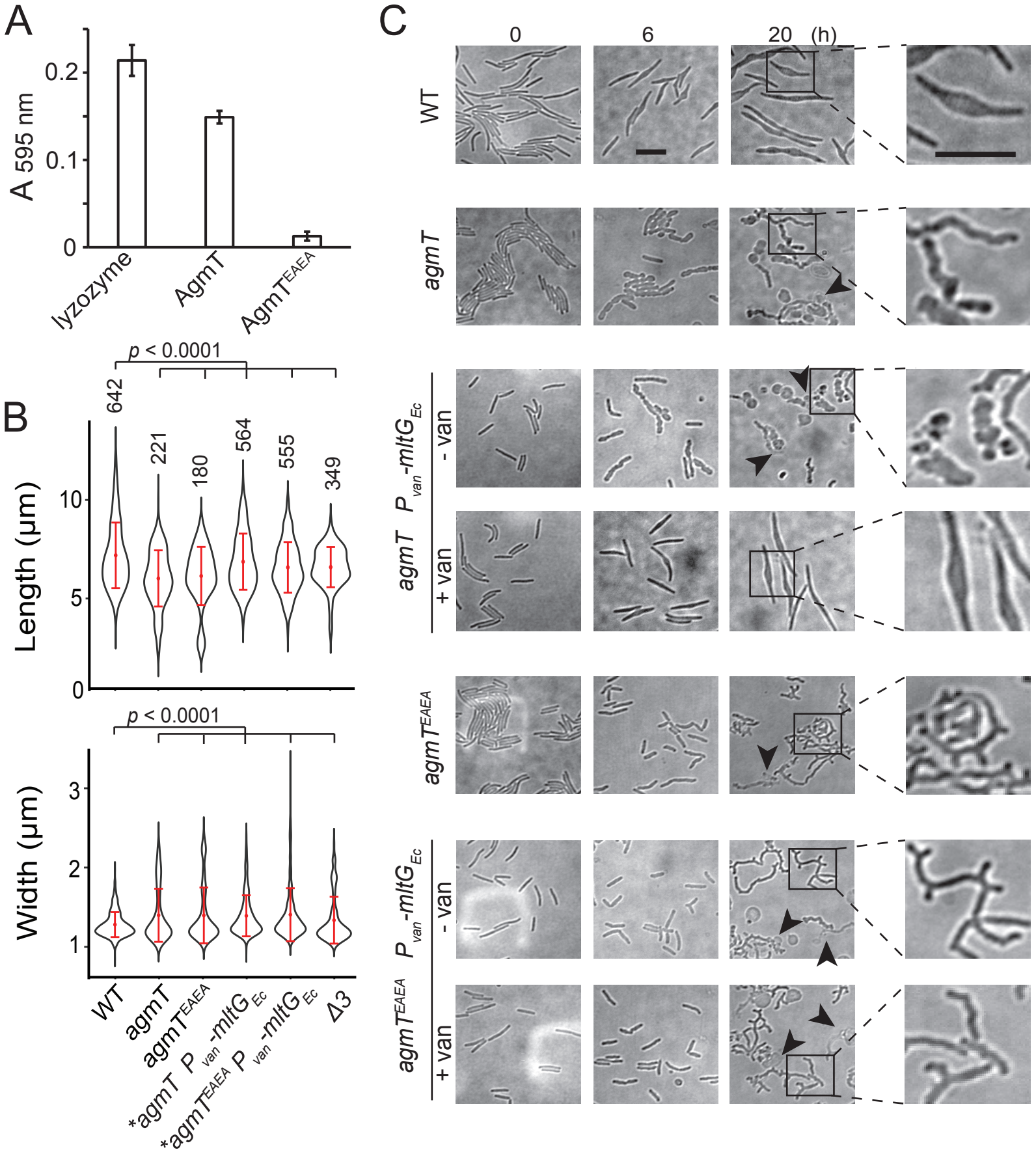
A
A 595 nm
0.2
0.1
0
lyzozyme
AgmT
AgmT^EAEA
B
p < 0.0001
642
221
180
564
555
349
Length (µm)
10
5
0
p < 0.0001
Width (µm)
3
2
1
WT
agmT
agmT^EAEA
*agmT P_van-mltG_Ec
*agmT^EAEA P_van-mltG_Ec
Δ3
C
0
6
20 (h)
WT
agmT
agmT P_van-mltG_Ec
- van
+ van
agmT^EAEA
agmT^EAEA P_van-mltG_Ec
- van
+ van

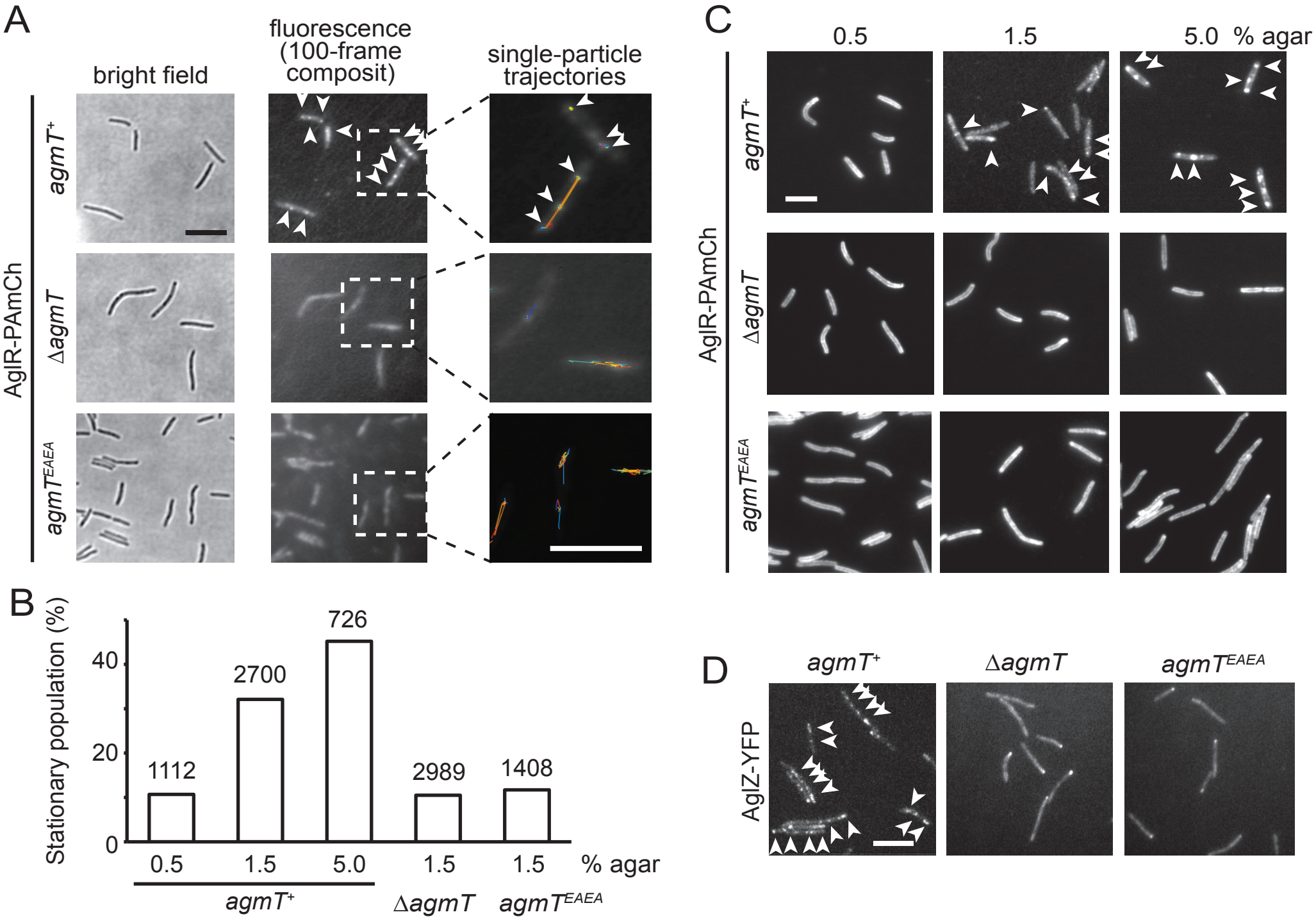
A
bright field
fluorescence (100-frame composit)
single-particle trajectories
AglR-PAmCh
agmT+
ΔagmT
agmTEAEA
B
Stationary population (%)
0
20
40
1112
2700
726
2989
1408
0.5
1.5
5.0
1.5
1.5
% agar
agmT+
ΔagmT
agmTEAEA
C
0.5
1.5
5.0 % agar
AglR-PAmCh
agmT+
ΔagmT
agmTEAEA
D
agmT+
ΔagmT
agmTEAEA
AglZ-YFP

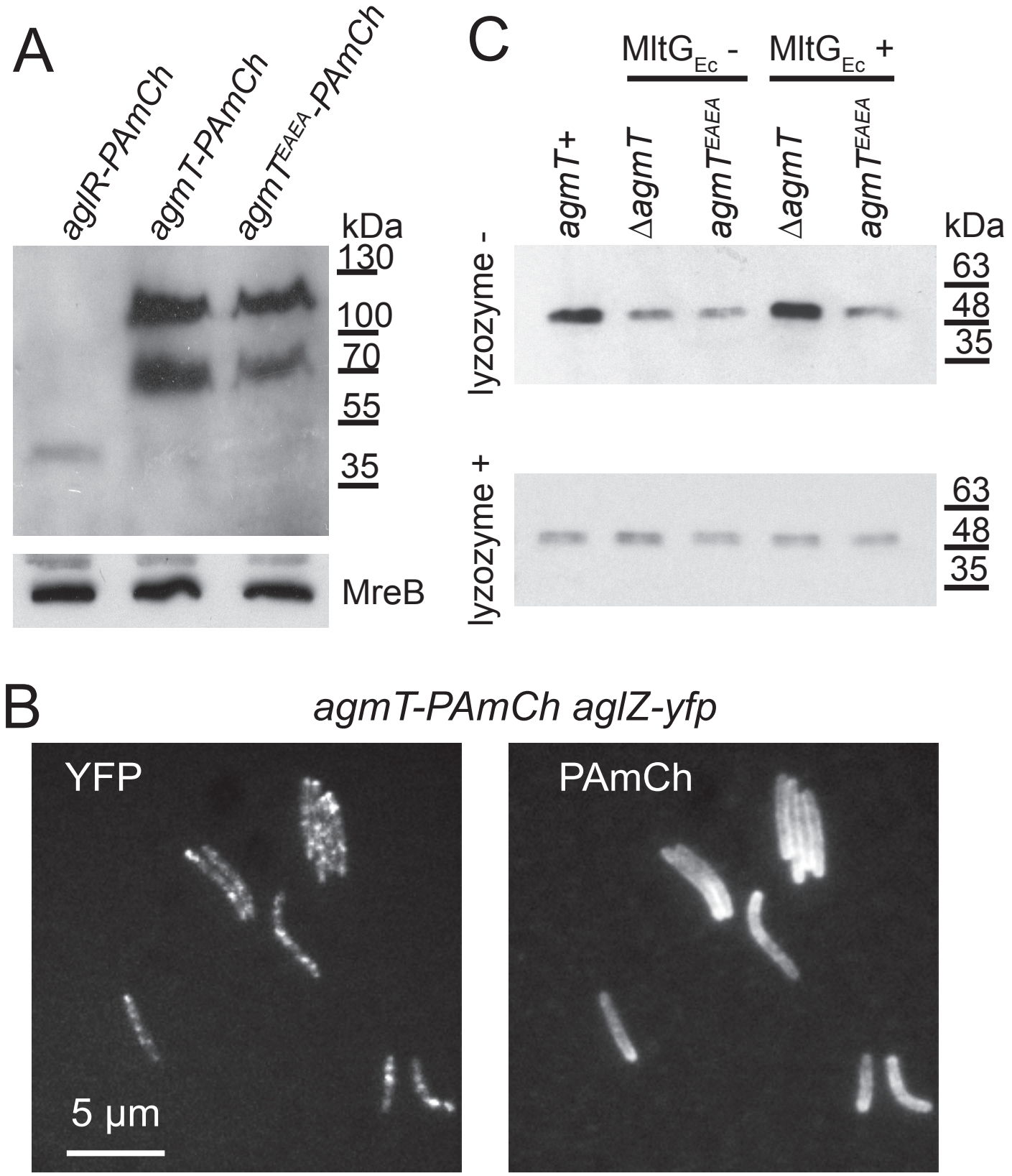
A
aglR-PAmCh
agmT-PAmCh
agmTEAEA-PAmCh
kDa
130
100
70
55
35
MreB
C
MltGEc -
MltGEc +
agmT+
ΔagmT
agmTEAEA
ΔagmT
agmTEAEA
kDa
lyzozyme -
lyzozyme +
63
48
35
63
48
35
B
agmT-PAmCh aglZ-yfp
YFP
5 µm
PAmCh